LAWRENCE
LIVERMORE
NATIONAL
LABORATORY

LLNL-TR-410644

Radiation-induced non-equilibrium redox chemistry of plutonium: implications for environmental migration

J. M. Haschke, W. J. Siekhaus

February 18, 2009

Disclaimer

This work performed under the auspices of the U.S. Department of Energy by Lawrence Livermore National Laboratory under Contract DE-AC52-07NA27344.

Radiation-induced non-equilibrium redox chemistry of plutonium: implications for environmental migration

John M. Haschke[1] *, Wigbert J. Siekhaus[2]

[1]Actinide Science Consulting, P.O. Box 96, Harwood, TX 78632 USA
[2] Lawrence Livermore National Laboratory, Livermore, CA 94550 USA
* To whom correspondence should be addressed. E-mail: johnhaschke@msn.com

This work performed under the auspices of the U.S. Department of Energy by Lawrence Livermore National Laboratory under Contract DE-AC52-07NA27344.

Abstract

Static concentrations of plutonium oxidation states in solution and at surfaces in oxide-water systems are identified as non-equilibrium steady states. These kinetically controlled systems are described by redox cycles based on irreversible disproportionation of Pu(IV), Pu(V), and Pu(VI) in OH-bridged intermediate complexes and at OH-covered oxide surfaces. Steady state is fixed by continuous redox cycles driven by radioactivity-promoted electron-transfer and energetically favorable reactions of Pu(III) and Pu(VII) disproportionation products with H_2O. A model based on the redox cycles accounts for the high steady-state [Pu] coexisting with Pu(IV) hydrous oxide at pH 0-15 and for predominance of Pu(V) and Pu(VI) in solution. The steady-state [Pu] depends on pH and the surface area of oxide in solution, but not on the initial Pu oxidation state. PuO_{2+x} formation is attributed to high Pu(V) concentrations existing at water-exposed oxide surfaces. Results infer that migration of Pu in an aqueous environment is controlled by kinetic factors unique to that site and that the predominant oxidation states in solution are Pu(V) and Pu(VI).

Introduction

Inconsistency of Pu redox chemistry with equilibrium control is evident for aqueous solutions and oxide-water systems. The dioxo ions of Pu(V) and Pu(VI) disproportionate despite unfavorable Gibbs energies [1] and oxide solubility is not described by equilibrium modeling [2,3]. Crystalline dioxide, PuO_2(c), is the stable oxide in water and pH-dependent dissolution as hydrolyzed Pu(IV) species is expected. However, steady-state Pu concentrations, $[Pu]_s$, are ~10^{10} higher than equilibrium values for PuO_2(c) and comparable to those for amorphous hydrous oxide, $Pu(OH)_4$(am) or $PuO_2 2H_2O$(am), formed by precipitation of Pu(IV) [2]. Data for the pH 0-15 range (Fig. 1a) show that $[Pu]_s$ values [4-8] are 10^2-10^4 greater than the equilibrium Pu(IV) concentration, $[Pu(IV)]_e$, for $Pu(OH)_4$(am) [9] and imply that PuO_2(c) is transformed into less-stable $Pu(OH)_4$(am), or that the dioxide and hydrous oxide are both transformed into another more-soluble (less-stable) phase [3,8]. More than 99% of the $[Pu]_s$ is present as Pu(V) and Pu(VI) [2], not as Pu(IV). The log$[Pu]_s$-pH results are especially perplexing because steady-state Pu concentrations decrease with increasing $[H^+]$ in the pH 1.5-3 range [2,5]. A proposed equilibrium description based on solubility control of $[PuO_2^+]$ by solid PuO_{2+x} accounts for $[Pu]_s$ in the pH 3-9 range [16], but does not account for spontaneous disproportionation of Pu(V) to Pu(IV) and Pu(VI) [1].

Reaction of PuO_2(c) with H_2O spontaneously forms H_2 and a high-composition oxide solid solution, PuO_{2+x}(c) ($0<x<0.27$) [10] containing Pu(IV) and Pu(V) [11]. Calculations show that PuO_{2+x} formation via the PuO_2+O_2 reaction is doubtful and that the observed PuO_2+H_2O reaction is energetically unfavorable [12,13]. Formation of PuO_{2+x} in the environment may enhance Pu solubility [3] and contribute to the surprisingly long

groundwater transport distances of 1.3 km at the Nevada Test Site (NTS) [14] and 3.9 km at the Mayak Production Association [15].

Here, disproportionation reactions, D_X, of aqueous hydroxo complexes with Pu(X) in intermediate oxidation states (X = IV, V, VI) are combined with Pu(X)-water reactions (X = III, VII) in defining non-equilibrium redox cycles. Static systems are described by steady-state cycles in which intermediate Pu(X) concentrations are fixed by equal rates of competing D_X reactions. These radioactivity-driven cycles describe the surface chemistry of water-exposed oxide and quantitatively determine the $[Pu]_s$-pH behavior of hydrous oxide-water systems.

Methods

Description of redox steady states is based on analysis of published data for solutions and solids. Digitization of data from graphical sources was facilitated by scanning and enlargement methods that limit the estimated errors (±5%) in dependent variables and have negligible effect on data evaluation or model development. Pu concentrations in Fig. 1a [4-8] are steady-state values coexisting with solids precipitated from acidic Pu(IV) nitrate solutions by dilution or NaOH addition. Disproportionation rates, R_{DX}, of Pu(X) [1,17-20] are described by the general equation: $R_{DX} = -d[Pu(X)]/dt = k_X[Pu(X)]^{nx}$, where $k_X = c_X[H^+]^{mX}$. Respective values of m_X and n_X define the numbers of protons (or OH^-) and Pu(X) ions involved in the rate-controlling step of D_X. Methods for deriving kinetic constants from [Pu(X)]-t data have been described previously [17].

Dependence of $[Pu]_s$ on the amount of Pu(IV) hydrous oxide coexisting with a steady-state solution is based on data showing a fifty-fold change in the apparent equilibrium quotient as the solid mass was varied from 1 mg l^{-1} to 5 g l^{-1} at pH 1.7±0.3

[2]. In the original study [21], steady states were reached with initial solutions of Pu(IV), Pu(V), or Pu(VI) and with mixtures containing Pu(IV) colloids. Equilibrium was defined by $2PuO_2^+(aq) + 2H_2O(l) \rightarrow Pu(OH)_4(am) + PuO_2^{2+}(aq)$. $[Pu]_s$ values for solutions with different amounts of solid are given by [Pu(V)+Pu(VI)] derived using $\{Pu\}_t$, the total moles (as solids and in solution) of Pu per liter, and the corresponding mole fractions of Pu(IV) from published ternary phase diagrams [21].

Definition of solution chemistry and modeling of $[Pu]_s$-pH results are guided by observation of one or more energetically unfavorable Pu(X) concentrations at steady state. Systems are apparently driven from equilibrium by energy from radioactive decay of Pu. Involvement of D_X reactions is suggested because they provide facile routes to all Pu(X) including Pu(VI). Since static Pu concentrations exceed equilibrium values, $[Pu]_s$ must be kinetically controlled and become fixed when the formation rate and the loss rate become equal for each Pu(X). Water is consistently present as solvent or adsorbate, inferring that H_2O actively participates in redox processes. The pH dependencies of k_X are correlated with those of $[Pu]_s$ and show involvement of polynuclear complexes with OH bridging groups that bind Pu(X) atoms and provide electron-transfer, ET, pathways for D_X reactions. Each linear segment in the $\log[Pu]_s$-pH data for hydrous oxide-solution systems (Fig. 1a) is consistent with control of the steady state by a unique D_X chemistry in that pH range.

Disproportionation kinetics

Disproportionation reactions of Pu(X) (Table 1A) transform Pu into all common oxidation states and ultimately determine the long-term aqueous redox chemistry of Pu. Equations in Table 1 are formulated to describe redox reactions for the entire pH 0-15

range. A single set of speciation-specific equations cannot be written because those reactions vary continuously with pH and because species are undefined for Pu(VII) and remain uncertain for other Pu(X). Whereas D_{IV} (Eq. 1A1) forms 2 Pu(III) and 1 Pu(VI) [17], D_V (Eq. 1A2) and D_{VI} (Eq. 1A3) are symmetric reactions with 1:1 product ratios [1,18]. As specified by Eq. 1A4, immediate reaction of the Pu(VII) product of D_{VI} with H_2O reforms Pu(VI) without detectable accumulation of the VII oxidation state and leaves Pu(V) as the only observed reaction product (Eq. 1A5). Kinetics of the Pu(VI)→Pu(V) transformation cannot be described by H_2O_2 reduction [18].

Formulation of D_X mechanisms is speciation-sensitive and rests on dependence of R_{DX} on [Pu(X)] and $[H^+]$ as defined by the general rate equation. Experimental values of m_X and n_X for Pu(X) (Table 2) are consistent with formation of hydroxo monomers and with their association as equilibrium di- or tri-nuclear complexes that are reactive intermediates in the rate determining steps of D_X reactions [1,17,18]. Below pH 4, hydroxo monomers of PuO_2^+ and PuO_2^{2+} form by protonation. Kinetic results infer that dimeric intermediates with single OH bridges form by association of PuO_2^+ and PuO_2^{2+} with their respective protonated ions [1,18]. Hydroxo monomers of Pu(IV) and those for Pu(V) and Pu(VI) above pH 4 form by hydrolysis and associate as polynuclear complexes. D_{IV} does not proceed by the accepted two-step bimolecular process, but via a single-step trimolecular reaction [17]. D_V and D_{VI} are bimolecular; k_V and k_{VI} (Table 2, Fig 1b) are from literature sources [1,17,18] and from evaluation of kinetic data [19,20].

If R_{DX} is determined by the pH-dependent concentration of a hydroxo complex of Pu(X), then k_X should be correlated with the concentration of Pu(X) hydroxo monomer. Thermodynamic data [22] show that the equilibrium $[PuO_2OH]$ is low in acidic media

and increases with pH until the equilibrium mole fraction of monomer approaches 1 near pH 10, the point beyond which a constant k_V is expected (Fig. 1b). Values of k_V decrease above pH 13 as the [PuO_2OH] is diminished by formation of $PuO_2(OH)_3^{2-}$ [23]. Values of k_{VI} (Table 2, Fig. 1b) are in close agreement with k_V. At Pu(VI) concentrations of interest, PuO_2^{2+} hydrolyzes first to PuO_2OH^+ below pH 6.5 and then to $PuO_2(OH)_2$ at pH 6.5-10 [22,24]. Facile dimerization of $PuO_2(OH)_2$ [24] suggests that D_{VI} remains bimolecular beyond pH 6.5. However, as shown by Eq. 2C3 (Table 2), a pseudo-first-order dependence on [H^+] is expected for pH 6.5-10 because the contribution to R_{DVI} from $PuO_2(OH)_2$ formation is negated by concurrent loss of PuO_2OH^+. Therefore, R_{DVI} is determined by reaction of the mixed dimer $(PuO_2OH\text{-}PuO_2(OH)_2)^+$ with $m_{VI} = 1$. The minimum in k_V near pH 4 coincides with the maximum in stability of aqueous Pu(V) [25] and is a consequence of low hydroxo monomer concentration. The mechanistic change from proton- to hydrolysis-driven D_V and D_{VI} reactions near pH 4 shows that PuO_2^+ and PuO_2^{2+} are amphoteric and suggests that oxide surfaces behave similarly.

D_{IV} is trimolecular in the pH 0-1 range where monomeric $Pu(OH)_y^{(4-y)+}$ (y = 0-4) species predominate, but the molecularity increases at higher pH [17]. If hydroxo trimers are the only reactive intermediates, n_{IV} should be fixed at 3 and k_{IV} should become constant as the mole fraction of $Pu(OH)_4(aq)$ approaches 1 at pH 7-8 [9]. Electron transfer in polynuclear hydroxo complexes and colloids of Pu(IV) undoubtedly contributes to D_{IV} above pH 1. Although Pu(IV) is formed reversibly by slow Pu(III)+Pu(VI) reaction below pH 0 [17,26], that reaction is negligible at higher pH where the concentration of Pu(III) is small and Pu(IV) is regenerated irreversibly via alternative D_X pathways.

Comparison of $\log[Pu]_s$-pH and $\log k_V$-pH curves (Figs 1a and 1b) shows that the pH dependence of $[Pu]_s$ is strongly correlated with that of k_V by an inverse square-root relationship over most of the pH range. The $\log[Pu]_s$-pH slopes have opposite sign and half the magnitude of the corresponding $\log k_V$-pH slope except for pH<1.5 and pH 6.5-10.

Radioactivity-promoted redox

In the classic description, redox reactions in solution are bimolecular processes driven by orbital overlap and finite probability of ET during molecular collision [27]. Trimolecular and higher-order reactions of D_{IV} [17] are not readily accommodated by that mechanism. Facile dimerization of PuO_2OH, PuO_2OH^+, and $PuO_2(OH)_2$, as well as formation of Pu(IV) hydroxo polymers, suggests that reactive intermediates are polynuclear species existing in equilibrium (or at steady state) with hydroxo monomers. Pu atoms in the polynuclear intermediates are bound by OH bridging groups that provide ET pathways for electron redistribution. A static non-equilibrium mixture of oxidation states forms as dinuclear and higher hydroxo intermediates with ET-altered electron distributions dissociate.

The proposed mechanism for OH-facilitated ET is based on x-ray photoemission spectroscopy (XPS) studies of water-exposed TiO_2 surfaces and identification of a hydrated-electron state involving the non-hydrogen-bonded H of bridging OH and chemisorbed H_2O [28]. The unoccupied 'wet-electron' state is populated by photo-induced ($h\nu$ = 3.05 eV) ET from Ti and is expected for other water-exposed transition metal oxides. Existence of similar states on bridging OH groups of aqueous hydroxo Pu complexes and population of those states by ET are implied by an intense band near

400nm (3.10 eV) in the absorption spectrum of Pu(IV) hydroxide polymer [29]. Studies with Pu(V) solutions show that D_V occurs in sunlight and in darkness [20], inferring that ET from Pu(V) to the hydrated-electron state is both photo- and radioactivity-induced. R_{DV} is twenty-fold faster in sunlight than in darkness. A broad spectrum of energy including E_X, the energy for exciting a Pu(X) electron to a hydrated electron state, apparently results as energy from radioactive decay (4.9-5.5 MeV alpha particles) is partitioned to Pu atoms in hydroxo complexes. D_X reactions are an inherent consequence of Pu-OH-Pu bonding and radioactivity-promoted ET to adjacent Pu atoms.

The surprisingly close agreement of c_X values for Pu(IV), Pu(V), and Pu(VI) in strong acid (Table 2) is consistent with promotion of ET in all D_X reactions by similar radioactivity-driven excitation of valence Pu electrons. D_V and D_{VI} undoubtedly proceed by excitation and transfer of single electrons in hydroxo dimers; coincidence of k_V and k_{VI} over a wide pH range (Fig. 1b) is unlikely if the reactions are driven by chemical potential. Formation of 2Pu(III)+Pu(VI) via a trimolecular D_{IV} mechanism involving simultaneous or sequential transfer of two electrons from one Pu(IV) in a hydroxo trimer is very improbable. Observations suggest a concerted process with formation of Pu(III) and Pu(V) by a one-electron transfer and immediate reaction of the Pu(V) product with the remaining Pu(IV) in the hydroxo trimer.

D_X-driven redox occurs via two competing processes: oxidative disproportionation, OD, and reductive disproportionation, RD. The oxidative process (Table 1B) is driven by the asymmetric D_{IV} reaction that forms Pu(III) and Pu(VI) in a 2:1 ratio. As shown by equations for aqueous Pu(IV) in a closed system, oxidation of product Pu(III) back to Pu(IV) by H_2O is necessary for OD. The reaction forms H_2, is energetically favorable

except at low pH [22], and occurs in Pu_2O_3 at near-neutral conditions and 25ºC [30]. Accumulation of Pu(VI) leads to D_{VI} and Pu(V) formation as product Pu(VII) is reduced back to Pu(VI) by H_2O [17]. The number of electrons lost by H_2 formation during Pu(III) oxidation is twice that produced by O_2 formation during Pu(VII) reduction. The net reaction (Eq. 1B2) transforms Pu(IV) into Pu(V)+OH^-.

Reductive disproportionation (Table 1C) initiates with onset of D_V as the Pu(V) product of OD accumulates in solution. Pu(IV) and Pu(VI) products are then consumed by continuing D_{IV} and D_{VI}. Steady-state concentrations, $[Pu(X)]_s$, with X = IV, V, and VI, are reached when the formation rate of each oxidation state equals its reaction rate. In the net reaction (Eq. 1C1), RD transforms Pu(V) into Pu(IV)+H^+. Approximately 23% of the Pu(VI) formed by D_{IV} at pH 0.7 is reduced directly to Pu(V) by H_2O (Eq. 1A5) [17], apparently due to promotion from residual energy in product Pu(VI) after ET. The directly reduced fractions of product Pu(VI) from D_{IV} and D_V are likely to increase and may approach 1 as the $1/2H_2O \rightarrow 1/4O_2 + H^+ + e^-$ reaction becomes increasingly favorable with increasing pH.

Absence of reaction in a closed system is implied by summing Eqs.1B2 for OD and 1C1 for RD, but that condition is not realized. Radioactivity-driven ET continuously forces D_X reactions from the minimum energy state and maintains non-equilibrium $[Pu(X)]_s$ values. At a given condition, indistinguishable steady states are expected regardless of initial Pu(X) because all common oxidation states appear in OD-RD. The process is best described as 'hybrid' because participating reactions are controlled by thermodynamics in some cases and kinetics in others. OD slows with decreasing pH due

to increasing stability of Pu(III), a product that accumulates as electrons from continuing RD are added to the redox system [17].

The preceding discussion applies to solutions without coexisting oxide or hydrous oxide solids. Low-pH solutions with relatively high $[Pu(IV)]_e$ are amenable to speciation studies if precipitation of Pu(IV) hydrous oxide is precluded by low $\{Pu\}_t$. Continuing RD without compensating OD progressively transforms high oxidation states to Pu(III) in solutions containing Pu(III), Pu(IV), plus Pu(VI) ([Pu] ~$1.8x10^{-4}$ M) at pH 0 and Pu(III), Pu(V), plus Pu(VI) ([Pu] ~$1.6x10^{-4}$ M) at pH 1 [26]. Precipitation of Pu(IV) hydrous oxide, the dominant reaction upon dilution of an acidic Pu(IV) stock solution to ~10^{-9} M in natural waters at pH 8.5, is followed by redistribution of Pu(X) in solution over a thirty-day period [31]. Pu remains in solution upon similar dilution of a Pu(VI) stock solution; Pu(IV) hydrous oxide precipitates as the [Pu(V)+Pu(VI)] is decreased by continuing RD over time.

OD-RD holds potential for markedly altering the redox chemistry of hydrous oxide and water-exposed dioxide. Pu atoms in bulk hydrous oxide, $Pu(OH)_4$(am) [32], and at the surface are bound by OH. Dissociative chemisorption of water during exposure of PuO_2(c) to H_2O(g) forms OH in the first monolayer [33]. Chemisorption of H_2O in the second layer is followed by reversible sorption of additional H_2O layers. The surface composition is $Pu(OH)_4$ for both Pu(IV) hydrous oxide and H_2O-exposed PuO_2 solids in solution and in vacuum. Extension of the OD-RD concept to these OH-covered oxides is logical because the network of surface Pu atoms and bridging OH groups resembles an extended polynuclear hydroxo complex of Pu(IV) on a substrate surface and beneath one

or more sorbed H_2O layers. Steady-state distributions of Pu(IV), Pu(V), and Pu(VI) are expected at hydroxo-coated surfaces as a result of OH-facilitated ET and OD-RD.

XPS data for the Pu $4f_{7/2}$ core level (Fig. 2a) show multiple Pu oxidation states at surfaces of hydrous oxides and water-exposed oxide [34], but identities and distributions of those states are not reported. In comparison to data for PuO_2 prepared in situ at 600ºC (Fig. 2aA), the spectrum for PuO_2 fired in air (Fig. 2aB) is broad and shifted toward higher binding energy, BE. Spectra for $PuO_{2.26}$ (Fig. 2aC) and Pu(IV) colloidal hydroxide (Fig. 2aD) are surprisingly similar and substantially shifted relative to PuO_2. The known presence of Pu(V) in $PuO_{2.26}$ [11] infers that the maximum near 427.0 eV is characteristic of Pu(V). The 1.5 eV spacing between this peak and BE for Pu(IV) [34] is identical to that for Pu(III) and Pu(IV) [35] and infers that BE for Pu(VI) in oxide is near 428.5 eV. A change in the oxidation-state distribution at the $PuO_{2.26}$ surface in vacuum is shown by a shift to lower BE over time (Fig. 2b).

Curve fitting shows that the $PuO_{2.26}$ XPS spectrum (Fig. 2c) is described by a sum of spectra for Pu(IV), Pu(V), and Pu(VI), the oxidation states expected for control by OD-RD. Results (Table 3) show that similar oxidation-state distributions exist in near-surface regions of colloidal hydroxide and $PuO_{2.26}$ despite differences in bulk composition and crystallinity. Existence of comparable steady-state concentrations of Pu(IV), Pu(V), and Pu(VI) on water-exposed surfaces implies that D_X rates are similar and is consistent with promotion of ET by transfer of decay energy to Pu atoms. Involvement of H_2O in OD-RD is inferred by predominance of Pu(IV) at adsorbate-free oxide surfaces formed by in-situ heating of $PuO_{2.26}$ (Fig. 2aA). Shifting and broadening of the spectrum for air-fired PuO_2

(Fig. 2aB) suggests that OD-RD was promoted by chemisorption of water during handling in air.

The spectral shift for aged $PuO_{2.26}$ toward that of dry PuO_2 (Fig. 2b, Table 3) and absence of an O 1s peak (BE = 533.3 eV) for chemisorbed H_2O after aging [34] are consistent with consumption of water and electron production via the Pu(VII)+H_2O reaction [17]. Spontaneous dehydration is reduction-driven and promoted by loss of product O_2 from the dynamically pumped XPS system and the resulting limitation on H_2+O_2 recombination (Table 1B). Steady state is maintained only if the system is closed or the H_2O source is unlimited. Curve-fitting shows that the PuO_2CO_3 spectrum [34] is described by a mixture of Pu(IV), Pu(V), and Pu(VI) plus Pu(VII) (Fig. 2d, Table 3). Disproportionation of Pu(VI) to Pu(V) and Pu(VII) is controversial [1], but occurrence of the D_{VI} reaction is confirmed by these results. Transformation of the PuO_2CO_3 surface to Pu(IV) oxide hydroxide after a year in ultra-high vacuum [34] is consistent with slow addition of electrons to the redox system by throttled reduction of Pu(VII) at the low concentration of residual H_2O in the oxide carbonate.

A diagram of OD-RD (Fig. 3) shows the pathways for forming steady-state products at the $Pu(OH)_4$ surfaces of hydrous oxide and water-exposed PuO_2. Constraint of the surface composition to a 4H:4O:1Pu ratio throughout the diagram describes behavior in vacuum and inexorably fixes the stoichiometry of the Pu(VII) product at $PuO_2(OH)_3$. The three oxidation states (IV, V, and VI) observed on OH-coated surfaces at steady state lie on the inner circle. Pu(IV) and Pu(V) are at the interface between the oxidative and reductive processes; D_{IV} drives OR to form Pu(V) and D_V drives RD to form Pu(IV). Attainment of equilibrium is precluded because Pu(IV), Pu(V), and Pu(VI) are

continuously formed and lost via radioactivity-driven disproportionation reactions. In addition to forming H_2, O_2, and H_2O, transient H and O produced at surfaces participate in a catalytic cycle that interfaces with OD-RD, incorporates O_2 into a system, and increases the oxidation rate of Pu metal in moist environments [10,33].

Formation of PuO_{2+x} and H_2 by the PuO_2+H_2O reaction and generation of H_2 during storage of moisture-exposed oxide [10] are apparently driven by the high steady-state Pu(V) activity maintained at OH-coated surface of PuO_2(c) by OD-RD (Table 3). A $[Pu(V)]_s$ of ~10 M exists in the surface zone comprised of two chemisorbed water layers and 50% Pu(V) in one crystallographic plane of oxide. Formation of PuO_{2+x} as a mixed-valance phase of Pu(IV) and Pu(V) is consistent with reduction of surface Pu(V) to Pu(IV) by electrons from Pu(IV) in bulk oxide and concurrent diffusion of O^{2-} into the lattice. Pu(III) formed by D_{IV} at the surface is oxidized back to Pu(IV) by H_2O. The net reaction forms PuO_{2+x} and H_2 (Table 1D). Failure to form PuO_{2+x} by PuO_2+H_2O in some cases [36] suggests that oxygen diffusion (or another essential step) was blocked, a condition that results in accumulation of H_2 plus O_2 and formation of H_2O via surface-catalyzed reaction [37]. The proposed oxidation of PuO_2 by H_2O_2 [13] is unlikely because peroxide is unstable at surfaces and reduces aqueous Pu(V) and Pu(VI) to Pu(IV) [9]. PuO_{2+x} formation is not observed in dry air or O_2 [10] because dissociative chemisorption of H_2O is essential for ET at oxide surfaces.

Modeling of steady states

Description of solutions coexisting with hydrous oxide is based on adaptation of the redox cycle to systems in which OD occurs only at $Pu(OH)_4$ surfaces and RD occurs only in the aqueous phase. The OD process (Fig.3) drives oxide dissolution by forming Pu(V)

at the solid surface and releasing that product into solution. RD transforms aqueous Pu(V) into Pu(VI) and Pu(IV) hydrous oxide. The OD and RD regimes are kinetically linked at steady state where the rates of Pu(V) release and Pu(IV) precipitation are equal. The steady-state formation rate of Pu(V) equals the loss rate and is independently defined by R, the rate of Pu(V) (or H) generation during PuO_{2+x} formation [10]. Pu(IV) and Pu(VI) are formed by D_V, but Pu(V) is the only net product of D_{VI}. Therefore, R_{DV} is twice R_{DVI} at steady state.

In solutions coexisting with hydrous oxide or PuO_2, $[Pu]_s$ is determined by the sum of $[Pu(IV)]_s$, $[Pu(V)]_s$, and $[Pu(VI)]_s$. Concentrations of Pu(III) (except at low pH) and Pu(VII) are negligible. Presence of Pu(IV) hydrous oxide fixes $[Pu(IV)]_s$ at $[Pu(IV)]_e$. $[Pu(V)]_s$ and $[Pu(VI)]_s$ are defined by $[Pu(X)]_s = (R_{DX}/k_X)^{1/nX}$. $R_{DV} = R$, $R_{DVI} = R_{DV}/2$, and $[Pu]_s$ is described as follows:

$$[Pu]_s = [Pu(IV)]_e + (CR/k_V)^{1/nV} + (CR/2k_{VI})^{1/nVI}. \quad (1)$$

The system-specific constant C ($m^2\ l^{-1}$) relates R_{DX} (mol $l^{-1}\ s^{-1}$) to R (mol $m^{-2}\ s^{-1}$) and shows that $[Pu]_s$ depends on A/V, the ratio of solid-area to solution-volume. The pH dependence of $[Pu]_s$ is incorporated by $k_X = c_X[H^+]^{mX}$. R is radioactivity driven and pH insensitive in both the oxide protonation and the hydroxylation regimes. However, a change in R is likely upon transition from protonated to hydroxylated oxide surfaces. Unless otherwise stated, the contribution of $[Pu(IV)]_e$ to $[Pu]_s$ (< 1%) is ignored.

The hybrid model is supported by data showing that derived equilibrium constants vary with the mass of Pu (IV) hydrous oxide per unit volume of solution at steady state [2]. If n_V and n_{VI} are equal (Table 2) and defined by n, and if C is replaced by the product of A_g ($m^2\ g^{-1}$) and g_l ($g\ l^{-1}$), the linear logarithmic form of Eq.1 is:

$$\log[Pu]_s = \log[(A_gR/k_V)^{1/n} + (A_gR/2k_{VI})^{1/n}] + 1/n \log(g_l). \quad (2)$$

Least-squares refinement of $[Pu]_s$-g_l data from measurements near pH 1.7 [2,21] gives $\log[Pu]_s = (-2.9\pm0.7) + (0.50\pm0.09)\log(g_l)$. As predicted by Eqn 2, $\log[Pu]_s$ is a linear function of $\log(g_l)$. As required by the bimolecular (n = 2) mechanisms of D_V and D_{VI}, the slope is 0.50.

A mirror-image correspondence of $\log[Pu]_s$-pH (Fig. 1a) and $\log k_V$-pH (Fig. 1b) curves is predicted by the hybrid model. Qualitatively, steady state is reached at low [Pu(V)] if k_V and k_{VI} are large and at high [Pu(V)] if they are small. If both m_X and n_X for Pu(V) and Pu(VI) have the same values (m and n) within the range of a linear $\log[Pu]_s$-pH segment, the derived $\log[Pu]_s$-pH form of Eq. 1 for that range is:

$$\log[Pu]_s = \log[(CR/c_V)^{1/n} + (CR/2c_{VI})^{1/n}] + m/n \text{ pH}. \quad (3)$$

For these cases, the hybrid model predicts that the $\log[Pu]_s$-pH slope is m/n as defined by kinetics of D_X. Observed slopes for the pH 1.5-3 and 3-6.5 regions (Fig. 1a) agree with predicted m/n values of 1/2 and -1, respectively (Table 2). Similar agreement for pH 10-13 (m/n = 0) and pH >13 (m/n = 2) implies that m_V equals m_{VI} within those ranges, or that the [Pu(VI)] is negligible due to facile Pu(VI)+H_2O reaction at high pH. Analysis shows predominance of Pu(V) in strongly basic solutions at steady state [7]. Deviation from Eq. 3 at pH 6.5-10 is expected because m_V does not equal m_{VI}. Contributions of $[Pu(V)]_s$ and $[Pu(VI]_s$ to $[Pu]_s$ are comparable [2] and an effective m/n of -3/4 is obtained by averaging -1 and -1/2 for the respective Pu(V) and Pu(VI) terms in Eq. 1 .

The $\log[Pu]_s$-pH slope of -3/2 at pH <1.5 disagrees sharply with the expected m/n of 1/2. Results are consistent with continuing RD maintenance of steady state in solution and with entry into a regime of oxide protonation and acid-driven dissolution. The pH

dependence of $[Pu]_s$ in strong acid is determined by the combined effect of $[H^+]$ on k_X and on the oxide dissolution rate described by $R' = k'[H^+]^4$ [38]. If R is replaced by $k'[H^+]^4$ in Eq. 1, the theoretical slope of $\log[Pu]_s$-pH at pH<1.5 is -(4-m)/n or -3/2.

Slopes and spans of linear $\log[Pu]_s$-pH segments are consistent with kinetic control of $[Pu]_s$, but validation of the hybrid model rests on quantitative prediction. Of eight requisite parameters (C, R, c_V, c_{VI}, m_V, m_{VI}, n_V, n_{VI}), all are known for pH 3-6.5 except C, a quantity fixed by g_l (~1.2 g l^{-1}) of $Pu(OH)_4$(am) added to test solutions [5] and by A_g of the solid at steady state. The hydrous oxide might be present as a single 1.3 mm-diameter sphere of ~10 g cm^{-3} density or as 10^7 10-μm-diameter spherules formed by continuous shaking of the solutions with A_g constrained to the 10^{-4}-350 m^2 g^{-1} range. On average, formation of 100-μm-diameter particles ($A_g = 4x10^{-3}$ m^2 g^{-1}) at steady state is reasonable and gives $C = 5x10^{-3}$ m^2 l^{-1}. Use of this value, kinetic parameters (Table 2), and R ($1x10^{-13}$ mol Pu(V) m^{-2} s^{-1}) at 25ºC [10] in Eq. 1 gives the line shown for pH 3-6.5 in Fig. 1a. The $\log[Pu]_s$-pH function is continuous and other linear segments are successively defined by extending the pH 3-6.5 result with slopes and termination points from kinetics. The resulting linear segments ($\log[Pu]_s = m/n\ pH + B$) in Fig 1a are defined by the following sets of pH range, m/n, and B: (<1.5, -3/2, -1.72), (1.5-3, 1/2, -4.72), (3-6.5, -1, -0.22), (6.5-10, -3/4, -1.84), (10-13, 0, -9.43), and (>13, 2, -35.34). Predicted steady-state Pu(V) and Pu(VI) percentages for pH 3-6.5 (59% and 41%, respectively) are in excellent agreement with average experimental values of 57% and 43% [5].

The decrease in $[Pu]_s$ with increasing $[H^+]$ for pH 1.5-3 (m/n = 1/2) is confirmed by measurements at different points on the test period [5], but Eq. 1 is accurate in this range only if CR is 500-fold larger than that for pH 3-6.5. A change in R is unlikely because

effects of oxide protonation first appear with onset of acid-driven dissolution below pH 1.5. The A_g (200 m^2 g^{-1}) derived from the intercept term of Eq. 2 and the $\log[Pu]_s$-$\log(g_l)$ intercept at pH 1.7 is 10^4 larger than for pH 3-6.5 and implies that the increase in $[Pu]_s$ is due to an A_g-driven increase in C.

A discrepancy exists in the transition point of $\log[Pu]_s$-pH from slope 1/2 to slope -1. Kinetic data (Table 2) indicate that the change is near pH 4, but $\log[Pu]_s$-pH results (Fig. 1a) show the transition near pH 3. [Pu] values measured shortly after addition of Pu(IV) hydrous oxide to aqueous solutions at pH 2-4 deviated from the -1 slope below pH 4, but the deviation point progressively shifted to pH 3 over a period of weeks as the slope for pH 1.5-3 reached 1/2 at steady state [5]. This result and a $\sim 10^2$ separation between $[Pu]_s$ values for high-surface-area hydrous oxide and low-surface-area PuO_2(c) microspheres [2] are consistent with the effect of A_g on $[Pu]_s$. A_g values derived from the intercept limits of the $\log[Pu]_s$-$\log(g_l)$ data for pH 1.7 (10 to 6×10^3 m^2 g^{-1}) agree with values calculated for spherical particles with diameters of 1μm to 1 nm. Formation of colloidal hydrous oxide accounts for the turbidity of low-pH solutions [8]. Sluggish attainment of steady state at pH 2-4 and the shift in pH of the transition point are consistent with slow transformation of the initial hydrous oxide to a high-surface-area solid/colloidal product.

As predicted by OD-RD, $[Pu]_s$ values measured in four pH 7.2 solutions with similar $\{Pu\}_t$, but different initial Pu(X) (X = III-VI), converged over time and agree with values in Fig. 1a [39]. The [Pu]-time curve for the Pu(IV) solution reached a minimum as $Pu(OH)_4$ precipitated near zero time and then increased over a two-day period until [Pu] exceeded $[Pu(IV)]_e$ by $\sim 10^4$ at steady state, a result that cannot be explained using the solubility model based on equilibrium control by Pu(IV) hydrous oxide.

Compiled $[Pu]_s$ values identified as 'solubilities of hydrated Pu(VI) oxide solids' for the pH 7.5-14 range [40] are somewhat higher than shown in Fig 1a, but are characterized by three linear log$[Pu]_s$-pH segments with slopes of -0.75, 0, and 2 in the respective pH ranges 7.5-10, 10-12.5, and 12.5-14. Regardless of the starting X, OD-RD apparently drives all solid-solution systems toward similar steady states at constant $\{Pu\}_t$ and pH. Specific areas of solid products tend to converge over time due to continuous dissolution of the solid phase and precipitation of Pu(IV) hydrous oxide in the OD-RD cycle, but some variations in $[Pu]_s$ are likely due to small changes in A_g with system age.

Except for pH and $\{Pu\}_t$ (or A/V), system variables have limited effect on the Pu concentration at steady state. $[Pu]_s$ decreases by a factor of three as temperature is increased from 25 to 90ºC at pH 7 [41]. Steady state was reached more rapidly with $^{238}PuO_2(c)$ than with $^{239}PuO_2(c)$ [8], but agreement of $[Pu]_s$ values for the two isotopes (Fig. 1a) suggests that isotopic state is unimportant. R_{DVI} is not altered by a high alpha-particle activity in a solution containing ^{210}Po [18]. $[Pu]_s$ values attained after a year in 2.5 M Cl^- solutions [39] agree with values reached more rapidly in low-ionic-strength, non-complexing media [2]. Average $[Pu]_s$ values for 1.0 m Na_2CO_3 are a factor of three larger than those for carbonate-free solutions at pH 12.5-15 [7], a result contradicted by other studies [6] and requiring further investigation. Although O_2 is preferentially consumed during PuO_{2+x} formation, the rates of formation in moist air, water vapor, and H_2-rich water vapor are indistinguishable [10], implying that the radioactivity-driven OD-RD cycle proceeds equally in both oxidizing and reducing systems.

Aqueous transport of plutonium

D_X reactions are slow and have limited effect on redox chemistry during aqueous Pu processing operations, but are likely to determine long-term behavior during migration of Pu in the environment. Downstream Pu at both NTS [14] and Mayak [15] is primarily associated with colloidal particles and colloid-facilitated migration in groundwater is proposed. The likelihood of kilometer-scale colloid transport in aquifers is uncertain [42] and the OD-RD-based description of Pu migration in the environment merits consideration.

Data (Fig. 1a) and model predictions imply that $[Pu]_m$, the concentration of Pu in water coexisting with hydrous oxide, will exceed $[Pu(IV)]_e$ if $\{Pu\}_t$ (or A/V) is large. Predominance of Pu(V) and Pu(VI) in solution is anticipated for both oxidizing and reducing systems. $Pu(OH)_4$(am) continuously dissolves via the OD process and re-precipitates as Pu(IV) is formed by RD. In groundwater systems, precipitation of hydrous oxide is expected on aquifer surfaces, including those of natural colloids, as a solution with high $[Pu(V)]_m$ and $[Pu(VI)]_m$ moves at the flow velocity. Analysis of samples from near the natural uranium reactor at Oklo shows ^{235}U enrichment consistent with migration, localized deposition in clay, and subsequent alpha decay of ^{239}Pu [43].

In addition to pH, A/V and the residence time of solid and aqueous phases (flow rate) are site-specific factors that determine $[Pu]_m$. Concentrations similar to $[Pu]_s$ of laboratory studies may form at sites like NTS where Pu sources are large and groundwater is limited. $[Pu]_m$ is expected to increase as A/V is increased by downstream deposition of high-surface-area hydrous oxide.

Marine systems have low A/V and $[Pu]_m$ values ($\sim 10^{-14}$ mol kg^{-1}) [44] that are substantially less than $[Pu(IV)]_e$. Average oxidation-state distributions for fresh and sea

waters (32% III+IV, 68% V+VI) and for rain water (34% III+IV, 66% V+VI) [20] are in remarkable agreement with Pu(X) distributions (30±5% IV, 70±5% V+VI) existing at surfaces of as-received $PuO_{2.26}$ and $Pu(OH)_4$ (Table 3). Marine solutions apparently form by leaching of ions from steady-state surfaces with slow alteration of resulting concentrations by subsequent redox. About 10^{-5} percent of the Pu(V) and Pu(VI) disproportionates per year at observed $[Pu]_m$ values and pH 7, if E_X is a constant fraction of radioactive energy at all $\{Pu\}_t$. Results also suggest that Pu is leached from hydrous oxide surfaces at the steady-state Pu(X) distribution existing prior to brief contact of a source with rain water. Contrary to earlier proposals [3,16], formation of PuO_{2+x} is not necessary for enhancement of $[Pu]_m$ by OD-RD.

Analyses of groundwater samples from downstream wells show Pu-containing colloids, but measured $[Pu]_m$ values ($\sim 10^{-14}$ M at pH 8.4) [14] are less than expected for solubility control by Pu(IV) hydrous oxide ($[Pu(IV)]_e \sim 10^{-11}$ M at pH >7, Fig. 1a). In addition to the likelihood of sample dilution by uncontaminated water during pumping, a change in A/V during collection is unavoidable and results in degradation of sample integrity over time. Observations are perplexing because $[Pu]_m$ should equal $[Pu(IV)]_e$ if hydrous oxide is present. Attainment of $[Pu(IV)]_e$ at steady state is sluggish for OD-controlled dissolution and is likely to be very slow at the low A/V of pumped groundwater samples.

Conclusions

Kinetic results are useful for following a reaction along the path toward the final chemical state, as well as for modeling the system. The potential for using kinetics in characterizing plutonium oxide-water systems has been recognized [3,25], but has

remained unutilized. Here, steady-state redox systems in the pH 0-15 range are described by a comprehensive kinetic model based on disproportionation of Pu in intermediate oxidation states.

Equilibrium methods have been consistently applied to plutonium redox chemistry despite failure to account for properties of steady-state systems. In a recent solubility study [16], log[Pu]-pH data are described by a line with -1 slope derived for equilibrium control of PuO_2^+(aq) by solid PuO_{2+x} (am, hyd)($x < 0.06$) in the pH 3-9 range. Failure to account for the high $[Pu(VI)]_s$ of steady-state solutions [2] or to predict $[Pu]_s$ outside the pH 3-9 range suggests that the model is inadequate. An equilibrium state with Pu(V) as the only oxidation state cannot exist at any pH because of D_V (Fig. 1b). Calculations based on $[Pu]_s$ [16] and kinetic data (Table 2) show that ~10% of the reported equilibrium [Pu(V)] is transformed to Pu(IV) and Pu(VI) per day at pH 9. Thermodynamic results show that PuO_{2+x} is unstable [12,13] and imply that higher oxide cannot participate in any true equilibrium process. The equilibrium description is based on reaction of PuO_2(am, hyd) with O_2 to form PuO_{2+x}, a product that is not obtained with ozone, atomic oxygen, or other strong oxidants [45]. Formation of PuO_{2+x} by O_2 only occurs via a catalytic cycle driven by reaction of PuO_2 with H_2O [10]. Restriction of equilibrium PuO_{2+x} compositions to low x values conflicts with observation of $PuO_{2.27}$ as the steady-state solid in near-neutral solution at 25ºC [10] and with the $PuO_{2.2}$ composition indicated [10] by the lattice parameter ($a_o = 0.5403$ nm) derived using x-ray diffraction data for the PuO_2-related phase existing at steady state [16].

Formation of non-equilibrium steady states in aqueous and plutonium oxide-water systems is contingent on three physicochemical factors. Multiple Pu oxidation states

allow D_X reactions to proceed. Bridging OH groups in polynuclear hydroxo complexes and at oxide surfaces provide requisite electron-transfer pathways for D_X. Radioactive decay of Pu isotopes is an essential energy source that drives ET in the absence of light. Electron excitation energies (E_{IV} ~300 kJ mol^{-1}) promote unfavorable reactions and maintain non-equilibrium states. A widely invoked concept of radiation-induced redox attributes non-equilibrium behavior to involvement of radiolytic products such as H_2O_2, but the approach fails to account for solution kinetics [1,18] or for PuO_{2+x} formation in water vapor [10]. In contrast, the spectroscopic, kinetic, and steady-state properties are consistent with radioactivity-induced D_X reactions in OD-RD.

Kinetic results give new insight into diverse aspects of plutonium chemistry. The slope change near pH 4 in the $\log k_X$-pH data for Pu(V) and Pu(VI) (Fig. 1b) implies that the dioxo cations are amphoteric. Formation of $PuOOH^{2+}$ and $PuOOH^{3+}$ promotes disproportionation of Pu(V) and Pu(VI) at low pH, creates zones of maximum stability for PuO_2^{+} and PuO_2^{2+} at minima in $\log k_X$-pH, and drives $[Pu]_s$ downward with increasing $[H^+]$ in the pH 1.5-3 range. The change from protonation to hydroxylation at pH 3-4 coincides with a large discontinuity in electrochemical potential of steady-state solutions coexisting with hydrous oxide [3]. Protonation of oxide surfaces below pH 1.5 is marked by a sharp increase in $[Pu]_s$ at low pH. Proportionality of the oxide dissolution rate to $[H^+]^4$ [38] infers that the solid phase in strong acid is PuO_2 and that Pu enters solution by forming $Pu^{4+}+2H_2O$. Formation of $PuO_2(OH)_3^{2-}$ as a stable Pu(V) complex in basic solution [23] is supported by kinetic results (Table 2) showing that the predicted $\log[Pu]_s$-pH slope ($m_V/n_V = 4/2$) equals the observed value of 2 at pH > 13.

Identification of the OD-RD cycle addresses the controversy over existence of PuO_{2+x} [12,13,36,46]. The non-equilibrium higher oxide does not form during exposure of PuO_2 to dry O_2 [46] because OH groups from sorption of water are essential for radioactivity-promoted ET. Both spontaneous formation by the PuO_2-H_2O [10] and thermodynamic instability [12,13] are properties of PuO_{2+x}. Formation of PuO_{2+x} at 350ºC [10] implies that the phase is kinetically stable over a sizeable temperature range. Gibbs energies of formation derived for the PuO_{2+x} solid solution [47] are invalid because H_2 pressures generated by the PuO_2+H_2O reaction are not equilibrium values. All thermodynamic data based on Pu(X) concentrations in steady-state solutions are of uncertain reliability.

Radioactivity-promoted ET and OD-RD-controlled dissolution are expected for actinide and other transuranium elements with multiple oxidation states and propensity for disproportionation. Like PuO_{2+x}(c), Np_2O_5(c) is unstable relative to NpO_2(c)+1/2O_2, but forms in water and becomes increasingly crystalline over time [40]. Slopes of log$[Np]_s$-pH data for NpO_2OH(am) at pH 6.5-13 correspond with those for log$[Pu]_s$-pH (Fig.1a) and imply that $[Np]_s$ is fixed by OD-RD. Despite an unfavorable Gibbs energy, H_2O oxidizes UO_2 under anoxic hydrothermal conditions [48]. Product U(VI) precipitates as schoepite, a hydrous oxide of UO_3, because D_{VI} and RD are precluded by absence of U(VII) as an accessible oxidation state. Observations suggest that daughter isotopes are released from water-exposed spent nuclear fuel as product H_2 escapes from an open system and UO_2 is progressively transformed into U(VI) hydrous oxide. ET-driven reactions may occur if oxides of transition metals with multiple oxidation states (e.g.; Ti, Cr, Mn) are exposed to moist radiation environments. Promotion of disproportionation by

sunlight and formation of hydrogen and oxygen via OD-RD suggests the possibility of collecting solar energy by direct dissociation of water.

Footnotes

1. J.M. Haschke, J. Nucl. Mater. 334 (2004) 225.
2. J.M. Haschke, R.L. Bassett, Radiochim. Acta 90 (2002) 505.
3. J.M. Haschke, V.M. Oversby, J. Nucl. Mater. 505 (2002) 187.
4. D. Rai, R.J. Serne, D.A. Moore, Soil Sci. Soc. Amer. J. 44 (1980) 490.
5. D. Rai, Radiochim. Acta 35 (1984) 97.
6. D. Rai, N.J. Hess, A.R. Felmy, D.A. Moore, M. Yui, P.Vitorge, Radiochem. Acta 86 (1999) 89.
7. C.H. Delegard, Radiochim. Acta 41 (1987) 11.
8. D. Rai, J.L. Ryan, Radiochim. Acta 30 (1982) 213.
9. R. Knopp, V. Neck, J.I. Kim, Radiochim. Acta 86 (1999) 101.
10. J.M. Haschke, T.H. Allen, L.A. Morales, Science 287 (2000) 285.
11. S.D. Conradson, B.D. Begg, D.L. Clark, C. Den Auwer, F.J. Espinosa-Faller, P.L. Gordon, N.J. Hess, R. Hess, D.W. Keogh, L.A. Morales, M.P. Neu, W. Runde, C.D Tait, D.K. Viers, P.M. Villella, Inorg. Chem. 42 (2003) 3715.
12. L. Petit, A. Svane, Z. Szotek, W.M. Temmerman, Science 301 (3003) 498.
13. P.K. Korzhavyi, L. Vitos, D.A. Andersson, B. Johansson, Nature Mater. Letters 3 (2004) 225.
14. A.B. Kersting, D.W. Efurd, D.L. Finnegan, D.J. Rokop, D.K. Smith, J.L. Thompson, Nature, 397 (1999) 56.

15. A.P. Novikov, S.N. Kalmykov, S. Utsunomiya, R.C. Ewing, R Horreard, A. Merkulov, S.B. Clark, V.V. Ykachev, B.F. Myasoedov, Science, **2006**, 314 (2006) 638.
16. V. Neck, M. Altmaier, A. Seibert, J.I. Yun, C.M. Marquardt, T. Fanghänel, Radiochim. Acta 95 (2005) 193.
17. J.M. Haschke, J. Nucl. Mater. 362 (2007) 60.
18. J.M. Haschke, J. Nucl. Mater. 340 (2005) 299.
19. A.D. Gel'man, V.P. Saitseva, Soviet Radiochem. 7 (1965) 58.
20. G.R. Choppin, J. Radioanal. Nucl. Chem., Articles 147 (1991) 109.
21. T.W. Newton, D.E. Hobart, D.P. Palmer, Radiochim. Acta 39 (1986) 139.
22. R. Guillaumont, T. Fanghänel, V. Neck, J. Fuger, D.A. Palmer, I. Grenthe, M.H. Rand, Update on the Chemical Thermodynamics of Uranium, Neptunium, Plutonium, Americium and Technetium, Elsevier, Amsterdam, Netherlands, 2003.
23. V.P. Shilov, Radiochem. 39 (1997) 328.
24. S.D. Reilly, M.P. Neu, Inorg. Chem. 45 (2006) 1839.
25. R. Guillaumont, A. Adolff, Radiochim. Acta 58/59 (1992) 53.
26. H. Capdevila, P. Vitorge, E. Giffaut, Radiochim. Acta 58/59 (1992) 45.
27. R.A. Marcus, J. Chem. Phys. 24 (1956) 966.
28. K. Onda, B. Li, J. Zhao, K.D. Jordan, J. Yang, H. Petek, Science 308 (2005) 1154.
29. D.A. Costanzo, R.E. Biggers, J.T. Bell, J. Inorg. Nucl. Chem. 35 (1973) 609.
30. J.M. Haschke, in: Transuranium Elements A Half Century, American Chemical Society: Washington, DC, 1992, pp. 416-425.
31. J.M. Cleveland, T.F. Rees, K.L. Nash, Nucl. Technol. 62 (1983) 298.

32. V. Neck, J.I. Kim, Radiochim. Acta 89 (2001) 1.

33. J.M. Haschke, J. Nucl. Mater. 344 (2005) 8.

34. J.D. Farr, R.K. Schulze, M.P. Neu, J. Nucl. Mater. 324 (2004) 124.

35. D.T. Larson, J. Vac. Sci. Technol. 17 (1980) 55.

36. P. Martin, S. Grandjean, M. Riper, M. Freyss, P. Blanc, T. Petit, J. Nucl. Mater. 320 (2003) 138.

37. J.M. Haschke, T.H. Allen, L.A. Morales, J. Alloys Compds. **2001**, 320 (2001) 58.

38. A.L. Uriarte, R.H. Rainey, Report ORNL-3695, Oak Ridge National Laboratory: Oak Ridge, TN, 1965.

39. H. Nitsche, K. Roberts, R. Xi, T. Prussin, K. Becraft, I. Al Mahamid, H.B. Silber, S.A. Carpenter, R.C. Gatti Radiochim. Acta 66/67 (1994) 3.

40. J. Fuger, H. Nitsche, P. Potter, M.H. Rand, J. Rydberg, K. Spahiu, J.C. Sullivan, W.J. Ullman, P. Vitorge, H. Wanner, Chemical Thermodynamics of Neptunium and Plutonium, Elsevier: Amsterdam, 2001.

41. D.W. Efurd, W. Runde, J.C. Banar, D.R. Janecky, J.P. Kaszuba, P.D. Palmer, F.R. Roensch, C.D. Tait, Environ. Sci. Technol. 32 (1998) 3893.

42. B.D. Honeyman, Nature 397 (1999) 23.

43. R. Bros, L. Turbin, F. Gautier-Lafaye, Ph. Holliger, P. Stille, Geochim. Cosmochim. Acta 57 (1993) 1351.

44. G.R. Choppin, A.H. Bond, P.M. Hromadka, J. Radioanal. Nucl. Chem. 219 (1997) 203.

45. J.M. Cleveland, The Chemistry of Plutonium, American Nuclear Society, La Grange Park, IL, 1979.

46. T. Gouder, A. Seibert, L. Havela, J. Rabizant, Surf. Sci. 601 (2007) L77.

47. J.M. Haschke, T.A. Allen, J. Alloys Compds. 336 (2002) 124.

48. Hj. Matzke, A. Turos, Solid State Ionics 49 (1991) 189.

Table 1. Reaction sequences in solution and in the adsorbed water layer on oxide[a]

A. Disproportionation reactions, D_X, of Pu(X) in intermediate oxidation states		(Ref.)
1A1	$3Pu(IV)\ (aq) + E_{IV} \rightarrow 2Pu(III)\ (aq) + Pu(VI)\ (aq)$	[17]
1A2	$2Pu(V)\ (aq) + E_{V} \rightarrow Pu(IV)\ (aq) + Pu(VI)\ (aq)$	[1]
1A3	$2Pu(VI)\ (aq) + E_{VI} \rightarrow Pu(V)\ (aq) + Pu(VII)\ (aq)$	[18]
1A4	$\underline{Pu(VII)\ (aq) + 1/2H_2O\ (l) \rightarrow Pu(VI)\ (aq) + H^+\ (aq) + 1/4O_2\ (g)}$	[18]
1A5	$Pu(VI)\ (aq) + 1/2H_2O\ (l) + E_{VI} \rightarrow Pu(V)\ (aq) + H^+\ (aq) + 1/4O_2\ (g)$	
B. Reaction sequence during oxidative disproportionation of Pu(IV) (closed system)		
	$3Pu(IV)\ (aq) + E_{IV} \rightarrow 2Pu(III)\ (aq) + Pu(VI)\ (aq)$	(1A1)
1B1	$2(Pu(III)\ (aq) + H_2O\ (l) \rightarrow Pu(IV)\ (aq) + OH^-\ (aq) + 1/2H_2\ (g))$	[22,30]
	$Pu(VI)\ (aq) + 1/2H_2O\ (l) + E_{VI} \rightarrow Pu(V)\ (aq)) + H^+\ (aq) + 1/4O_2$ (g	(1A5)
	$H^+\ (aq) + OH^-\ (aq) \rightarrow H_2O\ (l)$	
	$\underline{1/2H_2\ (g) + 1/4O_2\ (g) \rightarrow H_2O\ (l)}$	[37]
1B2	$Pu(IV)\ (aq) + H_2O\ (l) + E_{IV+VI} \rightarrow Pu(V)\ (aq) + OH^-\ (aq) + 1/2H_2\ (g)$	
C. Reaction sequence during reductive disproportiontion of Pu(V) (closed system)		
	$2Pu(V)\ (aq) + E_{V} \rightarrow Pu(IV)\ (aq) + Pu(VI)\ (aq)$	(1A2)
	$\underline{Pu(VI)\ (aq) + 1/2H_2O\ (l) + E_{VI} \rightarrow Pu(V)\ (aq) + H^+\ (aq) + 1/4O_2\ (g)}$	(1A5)
1C1	$Pu(V)\ (aq) + 1/2H_2O\ (l) + E_{V+VI} \rightarrow Pu(IV)\ (aq) + H^+\ (aq) + 1/4O_2\ (g)$	
D. Reaction sequence resulting in formation of $PuO_{2+x}(c)$[b]		
	$2x(PuO_2\ (c) + 2H_2O\ (ads) \rightarrow Pu(OH)_4\ (sur))$	[33]
	$2x(PuOH)_4\ (sur) + E_{IV+VI} \rightarrow PuO_2OH\ (sur) + H_2O\ (ads) + 1/2H_2\ (g))$	(1B2)
1D1	$\underline{(1\text{-}2x)PuO_2\ (c) + 2xPuO_2OH\ (sur) \rightarrow PuO_{2+x}\ (c) + xH_2O\ (ads)}$	
1D2	$PuO_2\ (c) + xH_2O\ (ads) + 2xE_{IV+VI} \rightarrow PuO_{2+x}\ (c) + xH_2\ (g)$	[10]

a. Excitation energies, E_X, derive from radioactive decay and are unique for each D_X. b. Layers containing Pu-OH on oxide surfaces are indicated by (sur).

Table 2. Identification of Pu(X) species and reactive intermediates from dependencies of D_X on [Pu(X)] and [H^+] at 25°C[a]

Eq.	pH Range	Speciation Reaction	m_X/n_X	Reactive Intermediate	c_X[b]
A. Pu(IV)					
2A1	<1.2	$Pu(OH)_y^{(4-y)+} + H_2O \leftrightarrow Pu(OH)_{y+1}^{(3-y)+} + H^+$	-3/3	$(Pu(OH)_3)_3^{3+}$ or $(Pu(OH)_4)_3^0$	$8x10^{-3}$
B. Pu(V)					
2B1	<4[c]	$PuO_2^+ + H^+ \leftrightarrow PuO_2H^{2+}$	1/2	$(PuO_2H\text{-}PuO_2)^{3+}$	$4x10^{-3}$
2B2	4-10	$PuO_2^+ + H_2O \leftrightarrow PuO_2OH + H^+$	-2/2	$(PuO_2OH)_2$	$4x10^{-15}$
2B3	10-13	$PuO_2OH + H_2O \leftrightarrow$ no reaction[d]	0/2	$(PuO_2OH)_2$	$4x10^{5}$
2B4	>13	$PuO_2(OH)_3^{2-} + 2H^+ \leftrightarrow PuO_2OH + 2H_2O$	4/2	$(PuO_2OH)_2$	$1x10^{56}$
C. Pu(VI)					
2C1	<4[c]	$PuO_2^{2+} + H^+ \leftrightarrow PuO_2H^{3+}$	1/2	$(PuO_2H\text{-}PuO_2)^{5+}$	$1x10^{-3}$
2C2	4-6.5	$PuO_2^{2+} + H_2O \leftrightarrow PuO_2OH^+ + H^+$	-2/2	$(PuO_2OH)_2^{2+}$	$4x10^{-15}$
2C3	6.5-10	$PuO_2OH^+ + H_2O \leftrightarrow PuO_2(OH)_2 + H^+$	-1/2	$(PuO_2OH\text{-}PuO_2(OH)_2)^+$	--

a. Data are from literature sourses [1,17,18]. b. Units of c_X vary with n_X and m_X so that the units of R_{DX} ($R_{DX} = k_X[Pu(X)]^{nx} = c_X[Pu(X)]^{nx}[H^+]^{mx}$) are mol l^{-1} s^{-1}. c. The terminal pH shifts from 4 to 3 when hydrous oxide is present. d. The mole fraction of PuO_2OH is 1 at pH 10-13 with R_{DV} and k_V constant ($m_V = 0$).

Table 3. Curve-fitting results of Pu $4f_{7/2}$ XPS spectra for oxides and hydrous oxides[a]

Sample	Fig./Curve	Calculated Oxidation State Percentage					FWHM[b]
		Pu(III)	Pu(IV)	Pu(V)	Pu(VI)	Pu(VII)	(eV)
PuO_2(c)	2a/A	5	90	5	--	--	1.83
$PuO_{2.26}$(c)[c]	2a/C, 2c	--	25	53	22	--	1.51
$PuO_{2.26}$(c, aged)[c]	2b/E	9	43	35	13	--	1.67
$Pu(OH)_4$(am)	2a/D	--	35	45	20	--	2.20
PuO_2CO_3(c)	2d	--	13	20	49	18	2.76

a. Digitized spectra [34] of samples at room temperature were analyzed using commercial curve-fitting software and the following BE values: III(424.0 eV), IV(425.5 eV), V(427.0 eV), and VI(428.5eV). The BE of 430.4 eV for Pu(VII) was fit in calculation. b. FWHM is the full width at half maximum. c. $PuO_{2.26}$ was analyzed in 'as received' condition (Fig. 2b/C) and after aging for an unspecified period in the spectrometer (Fig. 2b/E) [34].

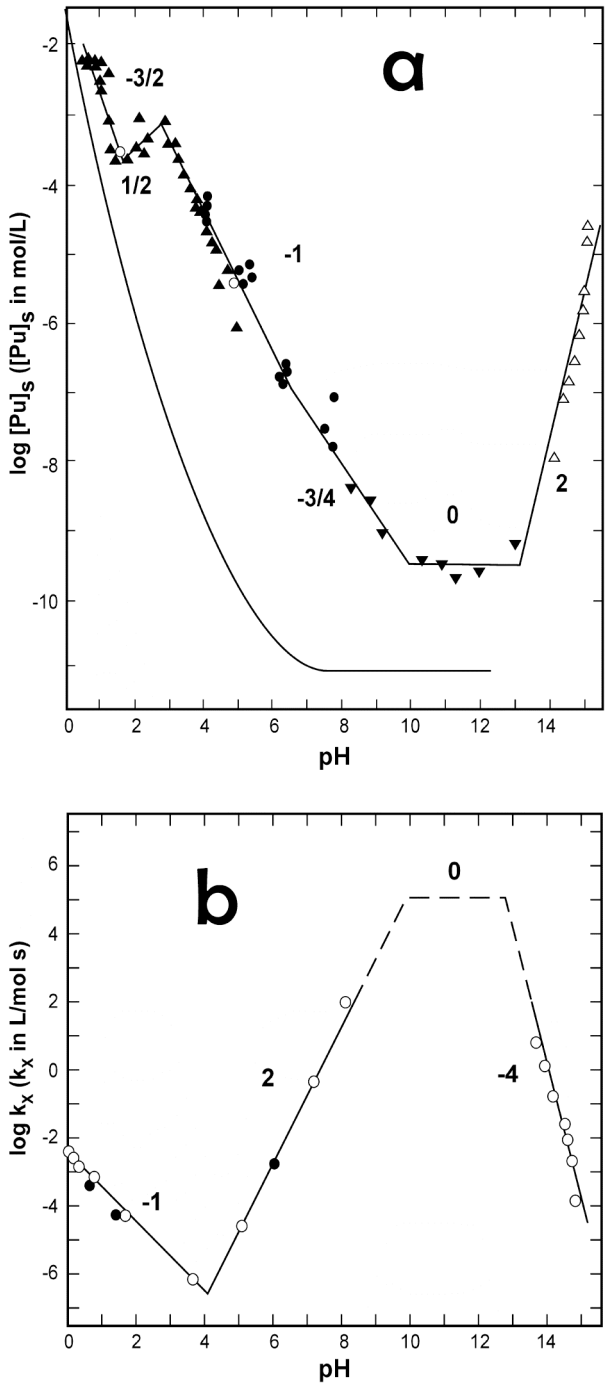

Figure. 1. The pH dependencies **(a)** of $[Pu]_s$ (data points) [4-8] and of $[Pu(IV)]_e$ (line without points) [9] coexisting with hydrous oxide in carbonate-free solutions and **(b)** of k_V (open circles) and k_{VI} (solid circles) [1,19,20]. All $[Pu]_s$ data are for ^{239}Pu except for the ^{238}Pu values at pH 1.5 and 4.8 (open circles) [8]. Ideal (integer and integer ratio) slopes are shown adjacent to linear log$[Pu]_s$-pH and logk_X-pH segments.

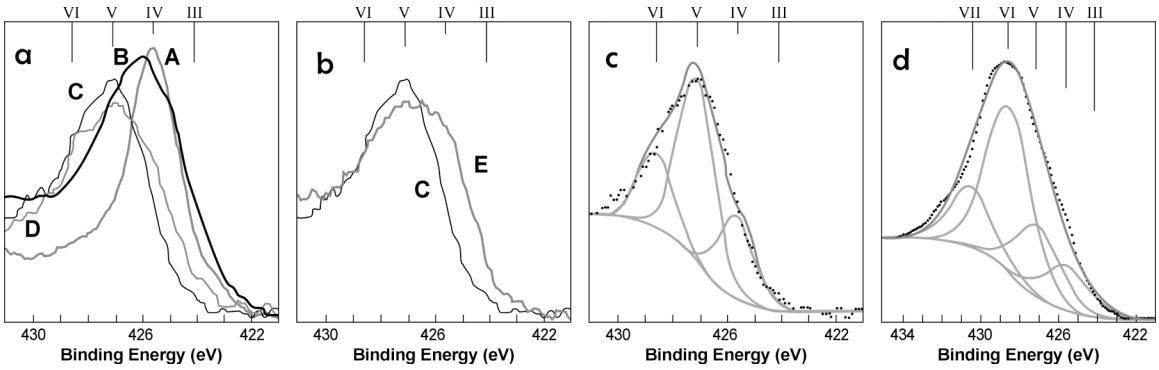

Figure 2. Pu $4f_{7/2}$ XPS spectra of plutonium oxides, hydrous oxides, and oxide carbonate [34]. **(a)** Curves are: A: in-situ-prepared PuO_2(c) (grey); B: air-fired PuO_2(c) (black); C: 'as- received' $PuO_{2.26}$(c) (dark grey); D: 'colloid-n' Pu(IV) hydroxide (grey). **(b)** Curves are: C: 'as received' $PuO_{2.26}$(c) (dark grey); E: aged $PuO_{2.26}$(c) (grey). **(c)** Fit of 'as received' $PuO_{2.26}$(c) spectrum (black dots). **(d)** Fit of PuO_2CO_3(c) spectrum (black dots).

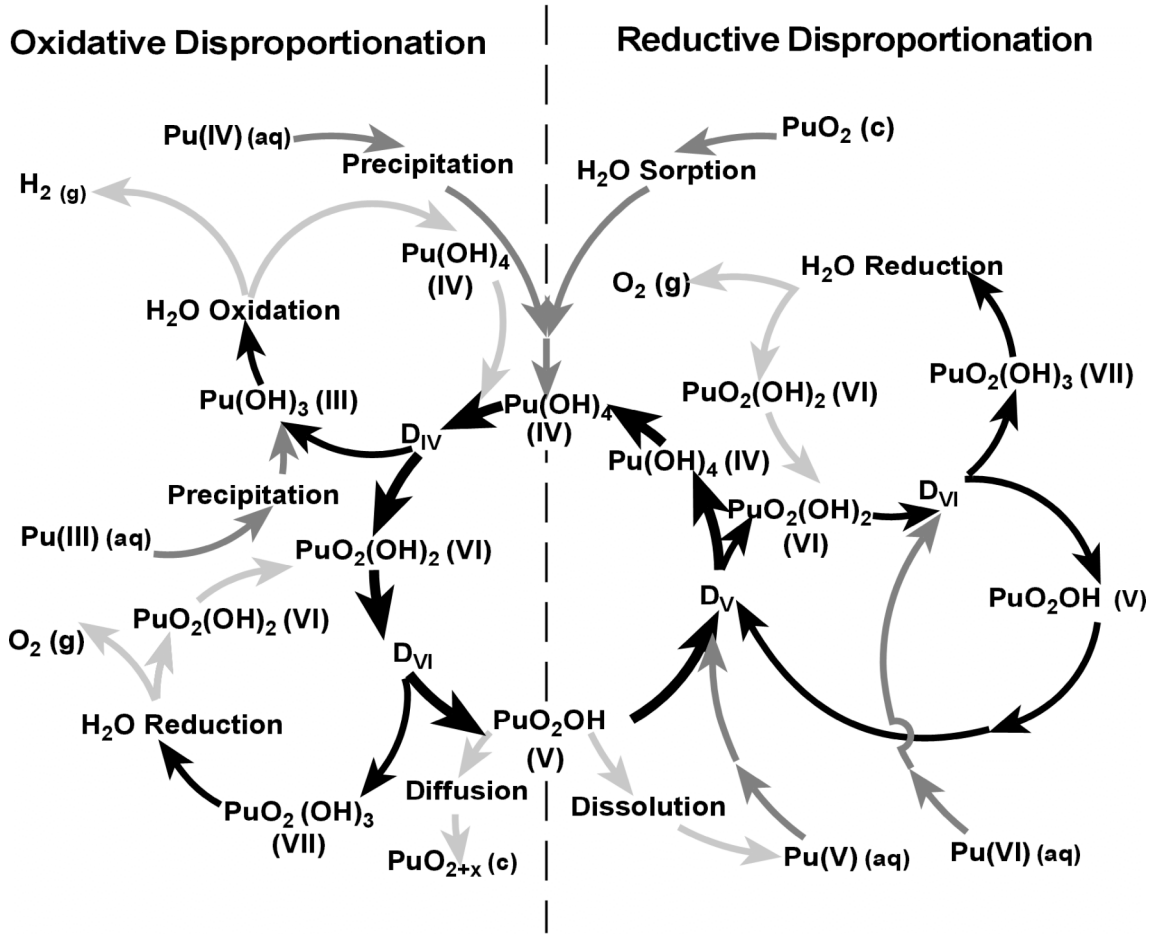

Figure 3. Cycle describing oxidative disproportionation of Pu(IV) and reductive disproportionation of Pu(V) at surfaces with the $Pu(OH)_4$ composition. Pathways of D_X reactions are shown by black arrows with the cycle core indicated by the inner circle of thick black arrows. Energetically favorable paths are shown by light grey arrows; entry paths for Pu with different oxidation states in solids and solutions are shown by dark grey arrows. Reaction stoichiometries are given in Table 1B and 1C.